Thickness dependence of $La_{0.7}Sr_{0.3}MnO_3/PbZr_{0.2}Ti_{0.8}O_3$ magnetoelectric interfaces

Jinling Zhou,[1] Vu Thanh Tra,[2] Shuai Dong,[3] Robbyn Trappen,[1] Matthew A. Marcus,[4] Catherine Jenkins,[4] Charles Frye,[1] Evan Wolfe,[1] Ryan White,[5] Srinivas Polisetty,[1,6] Jiunn-Yuan Lin,[2] James M. LeBeau,[7] Ying-Hao Chu,[8,9] and Mikel Barry Holcomb[1,a)]
[1]*Department of Physics and Astronomy, West Virginia University, Morgantown, West Virginia 26506, USA*
[2]*Institute of Physics, National Chiao Tung University, 30010 Hsinchu, Taiwan*
[3]*Department of Physics, Southeast University, 211189 Nanjing, China*
[4]*Advanced Light Source, Lawrence Berkeley National Laboratory, Berkeley, California 94720, USA*
[5]*National Institute of Standards and Technology, Gaithersburg, Maryland 20899, USA*
[6]*Department of Chemical Engineering and Material Science, University of Minnesota, Minneapolis, Minnesota 55455, USA*
[7]*Department of Materials Science and Engineering, North Carolina State University, Raleigh, North Carolina 27695, USA*
[8]*Department of Materials Science and Engineering, National Chiao Tung University, 30010 Hsinchu, Taiwan*
[9]*Institute of Physics, Academia Sinica, 105 Taipei, Taiwan*

(Received 27 July 2015; accepted 18 September 2015; published online 6 October 2015)

Magnetoelectric materials have great potential to revolutionize electronic devices due to the coupling of their electric and magnetic properties. Thickness varying $La_{0.7}Sr_{0.3}MnO_3$ (LSMO)/ $PbZr_{0.2}Ti_{0.8}O_3$ (PZT) heterostructures were built and measured in this article by valence sensitive x-ray absorption spectroscopy. The sizing effects of the heterostructures on the LSMO/PZT magnetoelectric interfaces were investigated through the behavior of Mn valence, a property associated with the LSMO magnetization. We found that Mn valence increases with both LSMO and PZT thickness. Piezoresponse force microscopy revealed a transition from monodomain to polydomain structure along the PZT thickness gradient. The ferroelectric surface charge may change with domain structure and its effects on Mn valence were simulated using a two-orbital double-exchange model. The screening of ferroelectric surface charge increases the electron charges in the interface region, and greatly changes the interfacial Mn valence, which likely plays a leading role in the interfacial magnetoelectric coupling. The LSMO thickness dependence was examined through the combination of two detection modes with drastically different attenuation depths. The different length scales of these techniques' sensitivity to the atomic valence were used to estimate the depth dependence Mn valence. A smaller interfacial Mn valence than the bulk was found by globally fitting the experimental results. © *2015 AIP Publishing LLC*.
[http://dx.doi.org/10.1063/1.4932517]

Magnetoelectric (ME) coupling refers to a material property where the internal magnetic (electrical) orders could be induced and controlled by external electrical (magnetic) fields.[1–6] Due to the likelihood that ME materials' domains can be switched and maintained at an atomic level with reduced energy cost,[7–11] faster, cheaper, and more sensitive devices could be built by upgrading current media with strong ME materials. Single-phase ME materials, however, are rare and suffer from significant drawbacks (i.e., weak ME coupling/low critical temperatures[12]). Strong ME coupling alternatively can occur at the interface of certain materials,[13–15] one of which is the interface between $La_{0.7}Sr_{0.3}MnO_3$ (LSMO) and $PbZr_{0.2}Ti_{0.8}O_3$ (PZT). $La_{1-x}Sr_xMnO_3$ exhibits a rich phase diagram[16,17] at varying doping level x. PZT is a strong room temperature ferroelectric (FE) material. In recent work on ME interfaces, a large magnetization modulation was found by Lu *et al.*[18] in $La_{0.67}Sr_{0.33}MnO_3$ by switching the FE polarization directions of a similar ferroelectric $BaTiO_3$ in $La_{0.67}Sr_{0.33}MnO_3$/ $BaTiO_3$ heterostructures. Vaz *et al.* reported a large magnetoelectric coefficient in a $La_{0.8}Sr_{0.2}MnO_3$/PZT bilayer and observed a change of Mn valence under external electric fields.[19] In addition to these observations, Mn valence is also known to associate with the LSMO magnetization.[20] Believing this interfacial valence modulation to potentially hold valuable information about the magnetoelectric coupling, we sought to investigate size effects on the interfacial Mn valence in magnetic LSMO layer in LSMO /PZT heterostructures.

With the independent increase of either PZT or LSMO thickness, the average Mn valence was found to increase in our systems. To separate the Mn valence at the interfacial layer with PZT from the bulk region of LSMO, we took advantage of the drastically different attenuation length of two techniques: valence sensitive[21] x-ray absorption in *L*-edge total electron yield (TEY) mode and *K*-edge fluorescence yield (FL) mode. The combination of these two modes is extremely useful for depth-dependence/interfacial studies and can be applied broadly to a wide range of heterostructures. Through the use of this method, we found an infusion

a)Author to whom correspondence should be addressed. Electronic mail: mikel.holcomb@mail.wvu.edu

 © 2015 AIP Publishing LLC

This article is copyrighted as indicated in the article. Reuse of AIP content is subject to the terms at: http://scitation.aip.org/termsconditions. Downloaded to IP: 223.3.79.249 On: Tue, 06 Oct 2015 14:19:21

of electron charges to the interfacial LSMO layer leading to an interfacial Mn valence smaller than the bulk (+3.3). As the interfacial layer becomes a smaller portion of the average signal as the film thickens, an increasing Mn valence with LSMO thickness is observed. As both our theory and experiments suggest, the independent increase of the Mn valence with PZT thickness, however, is due to the change of PZT polarization over the PZT thickness.[22]

To explain our experimental findings, a two-orbital double-exchange model[23] was used to simulate an LSMO (10 unit cell, ~4 nm)/PZT system with consideration of both the FE polarization and interface termination. Fig. 1 shows the results when the PZT polarization points towards LSMO. Because PZT polarization varies from 0 to approximately 100 μC/cm^2,[24] an equivalent surface charge Q of 0 to 1.0 e/u.c. area (e: electron charge; u.c.: unit cell) was applied to model the PZT polarization effect. Additionally, PZT has alternating $Zr_{0.2}Ti_{0.8}O_2$ and PbO planes. The $Zr_{0.2}Ti_{0.8}O_2$ termination plane (as shown in the inset of Fig. 1(a)) is referred to as n-type termination and a PbO termination as p-type. A neutral interface which is a mixture of half p-type and half n-type was also simulated for comparison. These planes are counted and labeled as the ith MnO_2 plane from the interface, where $i = 1, 2,\ldots,10$. The Mn valence was calculated from the Mn e_g charge density from each plane and is shown in Fig. 1(a) under four combined situations of surface charge and termination. The Mn valence near the interface (small i's) is suppressed due to the large PZT surface charge and gradually returns to nominal valence +3.3 near the 7th MnO_2 plane. While the simulated surface Mn valence ($i = 10$) is around 3.3 or larger, the surface is affected by the absence of apical oxygen coordination[25] and should be smaller due to higher $3z^2$-r^2 orbital occupancy than in the bulk.

Parameters that can be well predicted by this model are the Mn valences close to the interface. The interfacial valence modulation from n-type termination is relatively small compared to that from large PZT polarization/surface charge. Unlike the polarization effect whose direction can be flipped, the termination could not be reversed after growth.

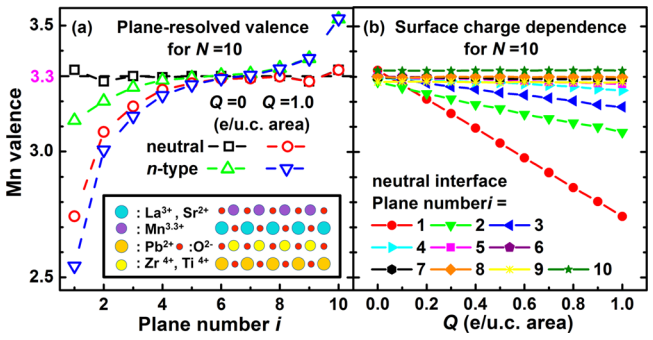

FIG. 1. (a) Model results for plane resolved Mn valence for thin film of LSMO with 10 MnO_2 planes grown on PZT. Both effects of surface charge Q (0 vs. 1.0 e/u.c. area, where e is the electron charge and u.c. stands for unit cell) and polar interface (neutral vs. n-type) are shown. Index i denotes the plane number counted from the interface. The inset illustrates the n-type interface. The nominal Mn valence of +3.3, based on the charge balance (70% $La^{3+}Mn^{3+}O_3^{2-}$ and 30% $Sr^{2+}Mn^{4+}O_3^{2-}$ in $La_{0.7}Sr_{0.3}MnO_3$), is marked in pink for comparison. (b) Mn valence behavior under varied surface charge Q with neutral interface.

Fig. 1(b) displays the simulated results of Mn valence at each MnO_2 plane under varied surface charges Q with neutral termination. The closer an MnO_2 plane is to the interface, the further the Mn valence is deviated from +3.3. The interfacial Mn valence also changes more when the polarization/surface charge is larger.

Based on the simulated results in Fig. 1(b), we developed a depth dependent Mn valence formula. Regardless of the strength of PZT surface charge, Mn valence was found to change exponentially from its interfacial value V_{int} to its valence V_{bulk} in the central LSMO. The Mn valence at a specific MnO_2 plane can be universally expressed as

$$V(z) = V_{bulk}\left[1 - \left(1 - \frac{V_{int}}{V_{bulk}}\right)\exp\left(-\frac{t-z}{L_i}\right)\right], \quad (1)$$

where L_i is the characteristic length at which the valence changes over the distance, t is the LSMO thickness (t_{LSMO}), and z is the distance from the LSMO surface to the specific MnO_2 plane. As seen in literature[29] and discussed earlier, the surface Mn valence is smaller than +3.3. Another exponential term is added to Equation (1) to better represent the depth dependent Mn valence

$$V(z) = \frac{V_{bulk}}{2}\left[1 - \alpha e^{-z/L_s}\right] + \frac{V_{bulk}}{2}\left[1 - \beta e^{-(t-z)/L_i}\right], \quad (2)$$

where α and β are the parameters that satisfy the boundary conditions $V(z=0) = V_{surf}$ and $V(z=t) = V_{int}$, V_{surf} is the Mn valence at the top MnO_2 plane, and L_s is the characteristic length over which the valence near the surface changes by 1/e. The behavior of L_i under different t_{LSMO} was checked by varying the lattice size in the simulations. Mn valence was found to exhibit similar values and changes at the same characteristic length L_i for $t_{LSMO} > 1.2$ nm at a constant PZT polarization.

The above theoretical results nicely explain most of our experimental observations. Several sets of measurements were made on two samples with small thickness gradients, though other similar samples and flat samples were also measured to verify consistency. The sample scheme was shown in Fig. 2 with exaggerated angles. Real samples have

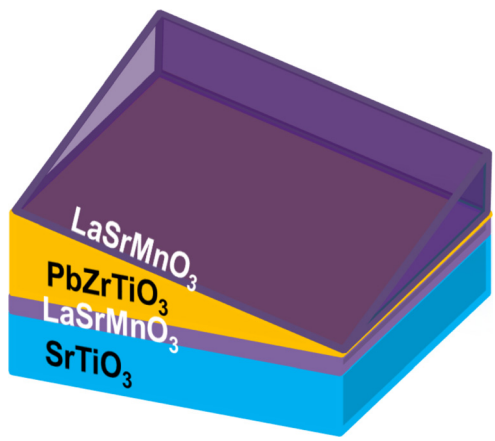

FIG. 2. Cartoon for the sample scheme. The orthogonal wedge directions of LSMO and PZT create a wide thickness range for both layers with reduced growth and measurement variations. The substrate is 1 mm thick, 5 mm × 10 mm wide; the thicknesses of all other layers are in nanometers.

This article is copyrighted as indicated in the article. Reuse of AIP content is subject to the terms at: http://scitation.aip.org/termsconditions. Downloaded to IP: 223.3.79.249 On: Tue, 06 Oct 2015 14:19:21

a t_{LSMO} from 0 to 3 nm in sample 1 and from 0 to 10 nm in sample 2. The PZT thickness (t_{PZT}) ranges from 0 to 300 nm for both samples over a length of 0.6 cm. The thickness gradient angles are smaller than 10^{-4} rad; thus, LSMO and PZT thickness is approximately constant over the μm spot sizes of the incident x-rays. This sample design provides a wide range of FM and FE layer thickness while greatly reduces growth and measurement variation, ideal for investigating size effects. Characterization and growth information are in the supplementary material.[26]

The Mn valence dependence on PZT thickness was studied in FL mode at beamline 10.3.2 of the Advanced Light Source (ALS). *K*-edge Mn x-ray absorption spectra (XAS) was measured at 0.4 nm, 1.2 nm, and 3.2 nm LSMO along the PZT thickness gradient. Mn valences are calculated by the linear combination method[21] and presented as three sets of data in Fig. 3. Below $t_{PZT} \sim 65$ nm, Mn valence increases with PZT thickness. Above $t_{PZT} \sim 65$ nm, Mn valences are relatively constant. This thickness dependence corresponds well with PZT domain changes in this thickness range[22] and is similar to the steep polarization changes observed at ultra thin PZT.[27] Piezoresponse force microscopy was taken along the PZT thickness gradient (supplementary material[26]). Thin PZT is monodomain. When the PZT becomes thicker, the ferroelectric domain directions transition from mostly out-of-plane (e.g., *c* domain) to polydomain (a mixture of *c* and in-plane *a* domains). Both domain structures are illustrated schematically in the inset of Fig. 3. Single domain PZT has a larger net surface charge. The surface charge for thick PZT with polydomain decreases as some domains will be aligned in the plane of the surface. Because the interfacial Mn valence changes in response to the PZT surface charge as shown in the simulation results in Fig. 1, the sharp increase of Mn valence with PZT thickness in our experiment is very likely due to the change of PZT polarization. This sensitivity of Mn valence to PZT polarization was further confirmed by poling PZT in opposite directions (supplementary material[26]).

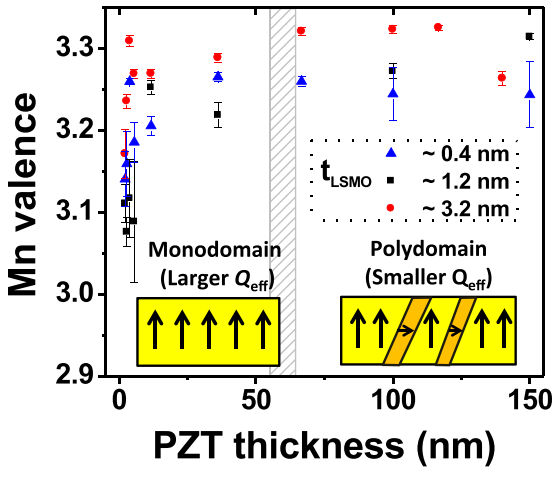

FIG. 3. Mn valence from Mn *K*-edge FL measurement vs. PZT thickness. The uncertainties are the standard deviations among varied linear combination results. The critical thickness for transition from monodomain to polydomain has been estimated and marked by the striped grey. The inset illustrates the correlation between PZT domain structures and surface charge.

In order to estimate experimentally the charge modulation on Mn at the LSMO/PZT interface, *L*-edge TEY and *K*-edge FL XAS are measured along the LSMO thickness gradient at a constant PZT thickness of 150 nm. TEY mode measures the yield of electrons escaping from the sample surface; FL mode collects the outgoing fluorescent light. Because the incident x-rays at the Mn *K*-edge are ten times more energetic than those at the Mn *L*-edge and the escape depth of FL photons is drastically larger than that of electrons, FL at Mn *K*-edge detects significantly deeper than TEY measurements at Mn *L*-edge.[28] For a rough estimation, the electron mean free path[29] predominantly determines the TEY attenuation length. The reported mean free path for Mn 3s electrons was about 0.5 to 1.8 nm at Mn *L*-edge energies.[30] The FL attenuation length is about 4 μm. After taking into account the grazing angles in measurements, the FL attenuation depth is about 0.2 μm. By taking advantage of this difference in depth contributions, the depth dependent and interfacial Mn valence could be estimated, as is elaborated in the following paragraphs.

Mn *L*-edge XAS in TEY mode was taken at 80 K and at a 30° grazing angle at beamline 6.3.1 of the Advanced Light Source in California. The empirical ratio method commonly used in electron energy loss spectroscopy[31] was adopted to determine the detected Mn valence for TEY measurements. The detailed procedure is included in the supplementary material.[26] Mn XAS from Gilbert *et al.*[32] were used as reference to establish the numerical relationship between Mn valence and L_3/L_2 ratio (shown in Fig. 4(a)). This established numerical relationship was then used to find the corresponding valence value from the L_3/L_2 ratio of the measured Mn XAS. The three Mn spectra in the inset of Fig. 4(a) were taken at different LSMO and PZT thickness. Their distinct fine structures demonstrate dissimilar Mn valences. These thickness dependent Mn valence values shown in Fig. 4(b) depend on the weighted contributions of the individual Mn valence from each MnO_2 plane. XAS in TEY mode result from the number of electrons escaped from the sample. Given the electron mean free path λ, the number of escaped electrons originating from depth z to $z+dz$ is proportional[33] to $\exp(-z/\lambda)dz$ where the depth z is the distance from the surface to the MnO_2 plane. If the LSMO thickness is t, the weighted contribution of the MnO_2 plane at depth z is $(\exp(-z/\lambda)dz)/(\int_0^t \exp(-z/\lambda)dz)$. The measured valence $\overline{V_{TEY}(t)}$ is

$$\overline{V_{TEY}(t)} = \frac{\sum_{i=1}^{t} V(z_i) \int_{z_{i-1}}^{z_i} \exp\left(-\frac{z}{\lambda}\right) dz}{\int_0^t \exp\left(-\frac{z}{\lambda}\right) dz}, \qquad (3)$$

where i stands for the i^{th} unit cell, Z_i is the distance from the surface to the unit cell center, and $V(z_i)$ is the Mn valence described in Equation (2).

To determine the depth dependence Mn valence values experimentally, *K*-edge Mn data with longer attenuation length are needed in addition to the surface sensitive *L*-edge Mn data. Mn *K*-edge XAS in FL mode[34] were taken at beamline 10.3.2 of the ALS. XAS from the buffer were subtracted from all measured fluorescence spectra for a direct

This article is copyrighted as indicated in the article. Reuse of AIP content is subject to the terms at: http://scitation.aip.org/termsconditions. Downloaded to IP: 223.3.79.249 On: Tue, 06 Oct 2015 14:19:21

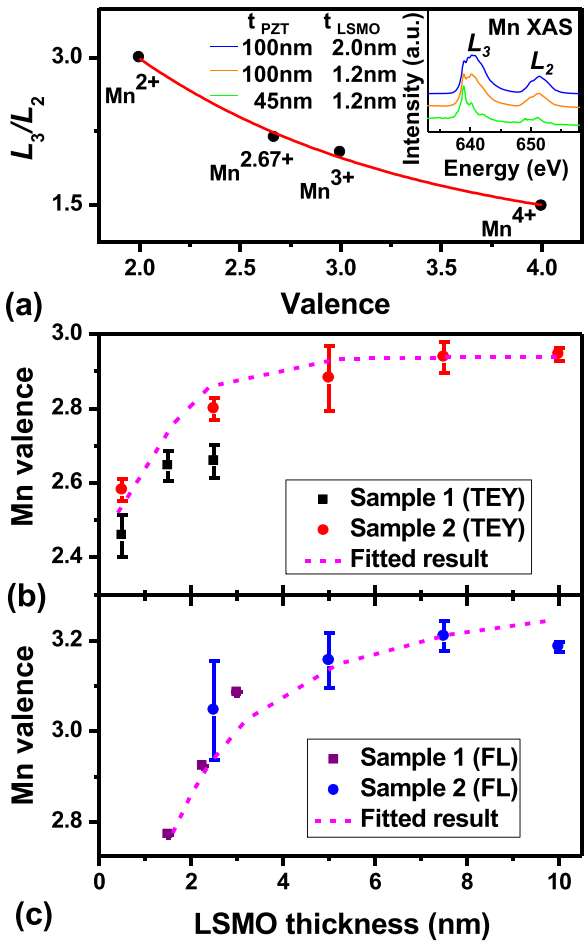

FIG. 4. (a) Relationship between Mn valance and L_3/L_2 intensity ratio (dots) established based on reference spectra from Ref. 31 with best fit line. The inset shows our Mn XAS spectra obtained in TEY mode. (b) Mn valence from TEY mode vs. LSMO thickness with the simulation curve. The uncertainties are estimated as the standard deviations among the results from repeated spectra at the same location. (c) Mn valence from FL mode vs. LSMO thickness with the simulation curve. Mn valence was calculated through linear combination of Mn reference spectra (Ref. 21). The uncertainties are the standard deviations among varied linear combination results.

comparison to the TEY results. Mn valences were obtained by fitting the linear combination of Mn reference spectra.[21] Because FL signal attenuates exponentially just as in TEY mode, Equation (3) was adopted for $\overline{V_{FL}(t)}$, where the FL attenuation length was used instead of the mean free path λ for TEY. Because the sample thickness is much less than the FL attenuation length, the contribution from each MnO_2 plane is approximately the same in the FL mode.

Depth dependent Mn valences were determined by globally fitting Equation (3) to the TEY and FL measurement results with valence formula from Equation (2). In the fitting procedure, all the parameters including the experimental mean free path λ, characteristic lengths L_i and L_s, and valence values V_{surf}, V_{bulk}, and V_{int} were allowed to change and were determined by searching for the smallest residuals. Our results suggest that L_s is larger than L_i. The fit resulted in a mean free path λ of approximately 2.5 u.c. = 1.0 nm, consistent with the electron mean free path in LSMO.[29] The best fit gave surface, interface, and bulk valences of $V_{surf} \approx 2.0$, $V_{int} \approx 2.52$, and $V_{bulk} \approx 3.36$. The best fit curves are shown in short dashed pink in Figs. 4(b) and 4(c). The fact that a better fit could not be achieved suggests that there is likely some thickness dependence in some of these parameters, such as the surface and interface valence and length scales. Based on our models and experimental data, such thickness dependence seems to mainly occur over the first few unit cells of the surface or interface and then saturate to a constant value, very similar to the experimental data shown line in Figs. 4(b) and 4(c). The deviation of the interfacial Mn valence from the bulk value indicates an interface charge reconstruction. This charge reconstruction confirms our theoretical simulation results and consistent with our experimental results of Mn valence dependence on PZT thickness. Shielding charges for PZT polarization add electrons to the interface region and lead to a smaller interfacial Mn valence. Polar discontinuity may also play a role although it is challenging to separate its contribution from the screening effects. Because electrons are attracted to the interface from the bulk region, the bulk Mn valence is slightly larger than 3.3.

In summary, thickness dependence studies of LSMO/PZT heterostructures were carried out by measuring Mn XAS along separate gradients of LSMO and PZT. Depth dependent Mn valence is established and fitted to the thickness dependent experimental data. Surface and interface Mn valences were found smaller than the nominal Mn value of +3.3. PZT surface charge and polar interfaces are two factors that lead to the deviation of interfacial Mn valence. Due to the linkage of Mn valence to LSMO magnetization, our research agrees with the work of others[19,35,36] that the screening of ferroelectric surface charge is likely the leading source of ME coupling at the interface. This hypothesis supports the report[37] that putting trapped charges in proximity of FM materials creates ME coupling effect. Our research also suggest single domain PZT is optimum for a large ME coupling effect to avoid in-plane domain structure. In addition to aiding the understanding of interfacial ME, deviations in interfacial valence also play an important role in exchange bias[38] and magnetic dead layers.[39] Because the influence of interfacial properties (such as atomic valence) has general implications well beyond the field of magnetoelectrics, depth dependent studies dramatically affect our ability to understand and enhance properties, and to explore interfacial phenomena.

The authors would like to thank Pavel Borisov and David Lederman for valuable discussions, and Benjamin Gilbert for providing the original data of Mn oxides. This work was supported by the WV Higher Education Policy Commission Research Challenge Grant No. HECP.dsr.12.29 and carried out at the Advanced Light Source, Lawrence Berkeley National Laboratory, Berkeley, CA, whose operations are supported by the Director, Office of Science, Office of Basic Energy Sciences, U.S. Department of Energy under Contract No. DE-AC02-05CH11231. Other characterization of the samples was completed at the West Virginia University Shared Research Facilities. Partial support for the work was provided by the National Science Foundation's ADVANCE IT Program under Award No. HRD-1007978. The double exchange model simulation by Shuai Dong was supported by the NSFC (Nos. 11274060 and 51322206). We also acknowledge the use of the

This article is copyrighted as indicated in the article. Reuse of AIP content is subject to the terms at: http://scitation.aip.org/termsconditions. Downloaded to IP: 223.3.79.249 On: Tue, 06 Oct 2015 14:19:21

Analytical Instrumentation Facility (AIF) at North Carolina State University, which is supported by the State of North Carolina and the National Science Foundation.

[1]W. Eerenstein, N. D. Mathur, and J. F. Scott, Nature **442**, 759 (2006).
[2]C. W. Nan, Y. H. Lin, and J. H. Huang, Ferroelectrics **280**, 153 (2002).
[3]N. Hur, S. Park, P. A. Sharma, J. S. Ahn, S. Guha, and S.-W. Cheong, Nature **429**, 392 (2004).
[4]X. Martí, F. Sánchez, J. Fontcuberta, M. V. García-Cuenca, C. Ferrater, and M. Varela, J. Appl. Phys. **99**, 08P302 (2006).
[5]R. Ramesh, F. Zavaliche, Y. H. Chu, L. W. Martin, S. Y. Yang, M. P. Cruz, M. Barry, K. Lee, P. Yang, and Q. Zhan, Philos. Mag. Lett. **87**, 155 (2007).
[6]V. V. Shvartsman, S. Bedanta, P. Borisov, W. Kleemann, A. Tkach, and P. M. Vilarinho, Phys. Rev. Lett. **101**, 165704 (2008).
[7]G. Lawes and G. Srinivasan, J. Phys. D: Appl. Phys. **44**, 243001 (2011).
[8]V. E. Wood and A. E. Austin, Int. J. Magn. **5**, 303 (1974).
[9]S. Priya, J. Ryu, C.-S. Park, J. Oliver, J.-J. Choi, and D.-S. Park, Sensors **9**, 6362 (2009).
[10]M. Bibes, J. E. Villegas, and A. Barthélémy, Adv. Phys. **60**, 5 (2011).
[11]J. Gao, Y. Wang, M. Li, Y. Shen, J. Li, and D. Viehland, Mater. Lett. **85**, 84 (2012).
[12]M. B. Holcomb, S. Polisetty, A. Fraile-Rodriguez, V. Gopalan, and R. Ramesh, Int. J. Mod. Phys. B **26**, 1230004 (2012).
[13]K. Dörr, C. Thiele, J.-W. Kim, O. Bilani, K. Nenkov, and L. Schultz, Philos. Mag. Lett. **87**, 269 (2007).
[14]J. P. Velev, S. S. Jaswal, and E. Y. Tsymbal, Philos. Trans. R. Soc. London, Ser. A **369**, 3069 (2011).
[15]H. J. A. Molegraaf, J. Hoffman, C. A. F. Vaz, S. Gariglio, D. van der Marel, C. H. Ahn, and J.-M. Triscone, Adv. Mater. **21**, 3470 (2009).
[16]S. Majumdar and S. van Dijken, J. Phys. D: Appl. Phys. **47**, 034010 (2014).
[17]J. Hemberger, A. Krimmel, T. Kurz, H.-A. Krug von Nidda, V. Yu. Ivanov, A. A. Mukhin, A. M. Balbashov, and A. Loidl, Phys. Rev. B **66**, 094410 (2002).
[18]H. Lu, T. A. George, Y. Wang, I. Ketsman, J. D. Burton, C.-W. Bark, S. Ryu, D. J. Kim, J. Wang, C. Binek, P. A. Dowben, A. Sokolov, C.-B. Eom, E. Y. Tsymbal, and A. Gruverman, Appl. Phys. Lett. **100**, 232904 (2012).
[19]C. A. F. Vaz, J. Hoffman, Y. Segal, J. W. Reiner, R. D. Grober, Z. Zhang, C. H. Ahn, and F. J. Walker, Phys. Rev. Lett. **104**, 127202 (2010).
[20]J. M. D. Coey, M. Viret, and S. von Molnár, Adv. Phys. **58**, 571 (2009).
[21]A. Manceau, M. A. Marcus, and S. Grangeon, Am. Mineral. **97**, 816 (2012).
[22]D. Kwon, B. Kim, B. G. Kim, and C. H. Chang, J. Korean Phys. Soc. **55**, 1327 (2009).
[23]S. Dong, X. T. Zhang, R. Yu, J.-M. Liu, and E. Dagotto, Phys. Rev. B **84**, 155117 (2011).
[24]I. Vrejoiu, G. L. Rhun, L. Pintilie, D. Hesse, M. Alexe, and U. Goesele, Adv. Mater. **18**, 1657 (2006).
[25]D. Pesquera, G. Herranz, A. Barla, E. Pellegrin, F. Bondino, E. Magnano, F. Sánchez, and J. Fontcuberta, Nat. Commun. **3**, 1189 (2012).
[26]See supplementary material at http://dx.doi.org/10.1063/1.4932517 for growth, sample characterization, data treatment, modeling, and poling results.
[27]V. Nagarajan, C. L. Jia, H. Kohlstedt, R. Waser, I. B. Misirlioglu, S. P. Alpay, and R. Ramesh, Appl. Phys. Lett. **86**, 192910 (2005).
[28]M. Kasrai, W. N. Lennard, R. W. Brunner, G. M. Bancroft, J. A. Bardwell, and K. H. Tan, Appl. Surf. Sci. **99**, 303 (1996).
[29]I. S. Tilinin, A. Jabloński, and B. Lesiak-Orlowska, Acta Phys. Pol. A **86**, 853 (1994), available at http://przyrbwn.icm.edu.pl/APP/PDF/86/a086z5p24.pdf.
[30]M. P. de Jong, I. Bergenti, V. A. Dediu, M. Fahlman, M. Marsi, and C. Taliani, Phys. Rev. B **71**, 014434 (2005).
[31]H. Tan, J. Verbeeck, A. Abakumov, and G. V. Tendeloo, Ultramicroscopy **116**, 24 (2012).
[32]B. Gilbert, B. H. Frazer, A. Belz, P. G. Conrad, K. H. Nealson, D. Haskel, J. C. Lang, G. Strajer, and G. De Stasio, J. Phys. Chem. A **107**, 2839 (2003).
[33]W. S. M. Werner, Appl. Surf. Sci. **235**, 2 (2004).
[34]M. A. Marcus, A. A. MacDowell, R. Celestre, A. Manceau, T. Miller, H. A. Padmore, and R. E. Sublett, J. Synchrotron Radiat. **11**, 239 (2004).
[35]S. Spurgeon, P. Balachandran, D. Kepaptsoglou, A. Damodaran, J. Karthik, S. Nejati, L. Jones, H. Ambaye, V. Lauter, Q. Ramasse, K. Lau, L. Martin, J. Rondinelli, and M. Taheri, Nat. Commun. **6**, 6735 (2015).
[36]J. Burton and E. Tsymbal, Phys. Rev. B **80**, 174406 (2009).
[37]U. Bauer, M. Przybylski, J. Kirschner, and G. S. D. Beach, Nano Lett. **12**, 1437 (2012).
[38]J. C. Rojas Sánchez, B. Nelson-Cheeseman, M. Granada, E. Arenholz, and L. B. Steren, Phys. Rev. B **85**, 094427 (2012).
[39]R. Hashimoto, A. Chikamatsu, H. Kumigashira, M. Oshima, N. Nakagawa, T. Ohnishi, A. Lippmaa, H. Wadati, A. Fujimori, K. Ono, M. Kawasaki, and H. Koinuma, J. Electron. Spectrosc. Relat. Phenom. **144**, 479 (2005).

This article is copyrighted as indicated in the article. Reuse of AIP content is subject to the terms at: http://scitation.aip.org/termsconditions. Downloaded to IP: 223.3.79.249 On: Tue, 06 Oct 2015 14:19:21